

Saving the Limping: Fault-tolerant Quadruped Locomotion via Reinforcement Learning

Dikai Liu^{1,2}, Tianwei Zhang², Jianxiong Yin¹ and Simon See¹

Abstract—Quadruped locomotion now has acquired the skill to traverse or even sprint on uneven terrains in remote uncontrolled environment. However, surviving in the wild requires not only the maneuverability, but also the ability to handle unexpected hardware failures. We present the *first* deep reinforcement learning based methodology to train fault-tolerant controllers, which can bring an injured quadruped back home safely and speedily. We adopt the teacher-student framework to train the controller with close-to-reality joint-locking failure in the simulation, which can be zero-shot transferred to the physical robot without any fine-tuning. Extensive simulation and real-world experiments demonstrate that our fault-tolerant controller can efficiently lead a quadruped stably when it faces joint failure during locomotion.

I. INTRODUCTION

Benefiting from the rapid advances in hardware and control algorithms, quadrupedal robots are becoming more intelligent in solving various tasks with high performance. They demonstrate high flexibility and versatility in complex contexts, and are expected to tackle many critical real-world missions, such as search & rescue [1], [2], patrol [3] and delivery [4].

Quadrupeds are normally deployed in uncontrolled remote environments [5], where accidents could happen at any time to cause potential critical hardware failures to the physical device, e.g., joint locking, free swinging. In such situations, it is important for quadrupeds to be robust against those hardware failures and come back home safely. Unfortunately, existing commercial quadrupeds are equipped with limited hardware failure detection and protection functions (e.g., overheating, signal losing), which are not sufficient to handle the motor failures. Prior studies have introduced solutions to achieve various locomotion tasks under *normal conditions*, such as traveling through rough terrains [5]–[7], jumping & falling recovery [8], high-speed running [9] and dexterous manipulation [10]. How to cope with hardware failures at runtime is still an unsolved problem, which is the focus of this paper.

It is challenging to grant the quadrupeds the capability of handling hardware failures automatically. Traditional control theory methods, like model predictive control (MPC) based controllers, require manual tuning of the model parameters with in-depth domain knowledge [11], [12]. The utilization of such pre-determined motion and trajectory planner is significantly restricted in the real world, especially when facing unknown environmental conditions and failures.

¹ NVIDIA AI Technology Centre (NVAITC), Singapore; e-mail: {dikail, jianxiongy, ssee}@nvidia.com

² School of Computer Science and Engineering, Nanyang Technological University, Singapore; e-mail: dikai001@e.ntu.edu.sg, tianwei.zhang@ntu.edu.sg



Fig. 1. Physical robot and its simulated counterpart used in our experiment. (a) Unitree A1 with our joint locking mechanism and UWB tag for indoor tracking. (b) Unitree A1 rendered in Isaac Gym simulator [13] with the official URDF model.

A more promising strategy is to apply reinforcement learning (RL) algorithms to train the policy in a simulator, and then transfer it to the physical world [6], [7], [9]. This can remarkably relax the requirement of domain knowledge. To improve the model performance in the real world, a number of simulators like Isaac Gym, have been developed with photo-realistic rendering and physical-accurate modeling [13]. Meanwhile, a lot of techniques have been proposed to reduce the sim-to-real gap [14]–[16]. Unfortunately, such gap remains in existence especially in the context of hardware failures, due to two reasons. First, it is impossible to simulate every possible environment state where the hardware failures could occur, even with the domain randomization technique [14]. Consideration of too many environment states can significantly slow down the training process, or even cause convergence failures. Second, the physical robot model used in the simulator is usually simplified, and cannot reflect the real robot conditions (e.g., with hardware faults).

Motivated by the above limitations, this paper presents the *first* methodology to improve the locomotion robustness of quadrupeds against potential hardware failures. We design a novel simulation strategy to realistically simulate joint locking failures, and a locking mechanism for real-world testing. We adopt the teach-student reinforcement learning paradigm to achieve jointly single-phase training and zero-shot transfer. The student model can efficiently extract information from onboard sensors. When deployed in a resource-constrained physical quadruped, the policy can provide real-time locomotion control against possible hardware failures in uncontrolled environments. We conduct extensive experiments in both simulation and a physical Unitree AI robot. Evaluations show that our method can significantly improve the robustness and hardware fault tolerance of RL-based control policies.

II. RELATED WORK

Quadruped Fault Tolerance. Despite the wide application of quadrupedal robots, there are very few works studying the fault-tolerant control [17]. Some papers considered the single joint locking failure, and adopted the traditional control theory to develop fault-tolerant gaits and inverse kinematics solutions [18]–[20]. A whole body control (WBC) method was recently proposed to optimize the posture [21]. However, most of these methods are designed for certain specific quadrupedal robots. With the recent trend of RL-based robotic controllers, Okamoto et al. [22] introduced a fault-tolerant RL algorithm. However, this solution is only tested on the Ant-v2 environment in the simulator, and its transferability to the physical world is unknown.

RL-based Quadruped Locomotion. Previous works introduced human-designed MPC controllers for quadrupeds to complete real-world applications [23], [24]. Recent research in reinforcement learning provides an alternative direction to the design of robotic controllers with less prior knowledge. For instance, Rudin et al. [25] adopted multiple types of rough terrains to improve the robustness of the quadruped agent. Kumar et al. [7] developed an adaption framework for locomotion. This framework was further extended in [9] to set a new world record for quadruped high-speed running. More advanced skills like wheel-based locomotion [26] and limb control [10] unveil the unlimited potential of RL algorithms for quadruped locomotion and control.

Sim-to-Real Gap in Robotic Control. The existence of sim-to-real gap [27], [28] has become a major obstacle for deploying RL-based algorithms. To reduce such gap, the most direct way is to conduct more physical-accurate and photo-realistic simulation [13] or use real data to tune the virtual model [29], which are not always available. Another common approach is to randomize parameters during simulation, which is known as domain randomization (DR) [14], [29]. Loquercio et al. [30] applied domain randomization on environmental texture for training a racing drone. Andrychowicz et al. [31] trained dexterous in-hand manipulation with random physical properties and object status. Chebotar et al. [32] used real-world information to tune the randomization of simulations. In quadruped locomotion, Tan et al. [29] applied random noise on sensor data, hardware specifications and environmental factors, which was widely adopted by subsequent works. Randomly generated terrains [6], [7], [25] are now commonly used to improve the policy robustness against different environments.

Teacher-Student Training. Online system identification predicts the underlying status, normally from a history of past states and actions [33] in robotics. Teacher-student framework is a common approach, where the teacher model leverages the privilege information for the student model to infer [6], [7]. The privilege information can be a combination of ground truth states like terrain map [5], [6], [34], and randomized domain parameters [7], [9]. The student model learns to imitate the teacher model from perceivable noisy sensor input like IMU, and joint encoders [7], [9] or with point cloud [5], [34].

III. METHODOLOGY

Our goal is to train a control policy π to guide the stable locomotion of the quadruped even when it faces hardware failures (e.g., joint locking). This policy takes as input the latent representation \hat{z}_t encoded from the perceivable sensor data, and outputs the desired joint position. It is designed to be capable of zero-shot deployment in the real world. Fig. 2 presents the overview of our methodology. Below we describe our methodology in detail.

A. Reinforcement Learning Architecture

We adopt the RL algorithm, which takes common onboard sensor data as observations, and outputs the optimal actions.

Observation. We collect the equipped low-level sensor data to provide observations. At any timestep t , motor encoders measure the joint position $q_t \in \mathbb{R}^{12}$ and velocity $\dot{q}_t \in \mathbb{R}^{12}$. IMU measures the orientation of the base body, which are further converted to the form of gravity vector $g_t^{ori} \in \mathbb{R}^2$ for roll and pitch. Force sensor data are binarized as the foot contact indicator $c_t \in \{0, 1\}^4$. We denote these available sensor data as $x_t = [q_t, \dot{q}_t, g_t^{ori}, c_t]$.

We follow the recent works [6], [7], [9] to generate the observations, which can capture the temporal information about the robot states. Specifically, the observation at the timestep t includes the current sensor data x_t and previous action a_{t-1} : $o_t = [x_t, a_{t-1}]$. Then we use the previous H observations ($[o_{t-H+1}, \dots, o_t]$) as the input to the controller.

Action. The control policy π predicts the target joint position $\hat{q} = a_t \in \mathbb{R}^{12}$, which is consequently processed by a PD controller for the desired torque of each actuator. In the real-word deployment, a_t is directly passed to the robot onboard controller. In the simulation, a generic PD controller is implemented as follows to compute the torque τ ,

$$\tau = K_p(\hat{q} - q) + K_d(\dot{\hat{q}} - \dot{q})$$

where K_p and K_d are the stiffness and damping gain controlled by domain randomization (Section III-D) and the target joint velocity $\dot{\hat{q}}$ is set to 0.

Reward Function. Closely following [7], [9], the reward functions encourage the agent to move forward stably and smoothly with a reasonable high speed. Details of each reward term can be found in Table I

To prevent the training from collapsing at an early stage, we adopt the strategy in [7], [16], where a small multiplier k_t is applied to certain penalty terms to allow for more aggressive exploration. This multiplier is initialized as $k_0 = 0.08$, and scaled with a fixed curriculum $k_{t+1} = k^{0.997}$.

B. Joint Teacher-Student Framework

Our goal is to obtain a zero-shot policy, which is trained completely in the simulator and transferred to the real world without fine-tuning. For RL-based policy, leveraging the privileged underlying states of the robot and environment can yield better performance under a smaller number of training iterations [35], [36]. We adopt the teacher-student learning paradigm [6], [7], [9] to achieve this goal. This learning

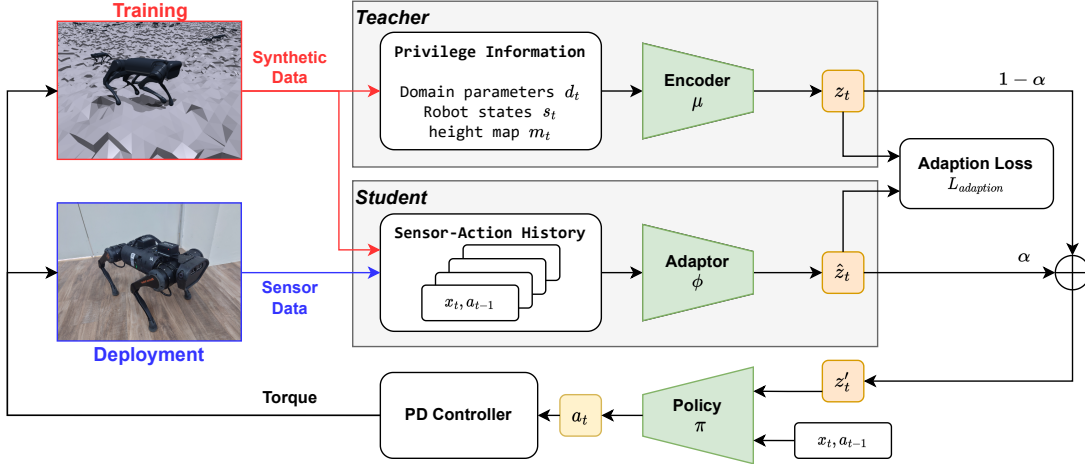


Fig. 2. Overview of our methodology. We adopt the reinforcement learning architecture with the teacher-student framework leveraged from prior work [7], [9] to train the policy. The architecture consists of a teacher network, a student network and a policy network. During training, synthetic data from the simulator is used to compute the latent representation z_t and \hat{z}_t from the teacher and student respectively. By fusing the latent information, all the three networks are trained jointly for fast convergence in the early stage and an optimized student-policy in the end. The resulted policy and student model will be directly deployed on the physical robot without any further fine-tuning.

TABLE I
REWARD TERMS IN OUR RL TRAINING METHODOLOGY

Category	Term	Formula	Scaling
Movement	Forward	$\min(v_t^x, 0.5)$	1.0
	Lateral movement	$\ v_t^y\ ^2$	-1.5
	Yawing	$\ \omega_t^z\ ^2$	-0.5
Stability	Base bumping	$\ v_t^z\ ^2$	-2.0
	Base rolling	$\ \omega_t^{x,y}\ ^2$	-0.02
	Base orientation	$\ g_t^{x,y}\ ^2$	-1.0
	Joint off limit	$\mathbb{1}_{q > q_{max}} \ q - q_{min}\ $	-10.0
	Collision	$\mathbb{1}_{collision}$	-1.0
Smoothness	Joint acceleration	$\ \dot{q}_t - \dot{q}_{t-1}\ ^2$	-1.0e-8
	Power consumption	$\int_{t-1}^t \ \tau \cdot \dot{q}\ dt$	-5.0e-3
	Feet air time	$\sum(t_{air} - 0.5)$	1.0

framework enables implicit system identification of hidden environmental and robot dynamics e_t for different behaviours. It can learn to infer the dynamics from perceivable data, making the policy deployable in the real world.

Specifically, a teacher model μ is introduced to encode the environmental factor e_t into the latent space representation z_t with length D :

$$z_t = \mu(e_t) \in \mathbb{R}^D$$

To better capture the dynamics, e_t should contain necessary underlying ground-truth synthetic data that are accessible from the simulator. We design e_t to include the domain parameters d_t (Section III-D), clean robot states $s_t = [v_t, \omega_t]$ and height map m_t of the surrounding terrain.

A student model ϕ is also introduced to learn from the past H observations $[o_{t-H+1}, \dots, o_t]$ to mimic the encoding from the teacher model μ . By performing system identification, ϕ predicts the dynamics in the same latent space:

$$\hat{z}_t = \phi(o_{t-H:t})$$

Previous works only jointly optimize the control policy and teacher model, while training the student model separately [6], [7], [9]. This adaption training only focuses on imitating teacher model's behaviors. Let us denote the control policy from such method as π_T . During policy optimization, the actions are

$$a_t = \pi_T(z_t, o_t) = \pi_T(\mu(e_t), o_t)$$

The control policy π_T can be unrolled for offline supervised optimization [6], [7], or on-policy data can be utilized for separate online adaption optimization [9]. The final deployment model directly reuses π_T for encoded sensor information:

$$a_{deployment} = \pi_T(\hat{z}_t, o_t) = \pi_T(\phi(o_{t-H:t}), o_t)$$

To imitate teacher model's behaviour, we need to minimize the loss function $\mathcal{L}_{adaption} = \|z_t - \hat{z}_t\|^2$. However, it is almost impossible to mimic an exact latent representation from the student to make $\hat{z}_t = z_t$, especially for certain corner cases. Since π_T is only optimized against the teacher's latent representation z_t , any small difference between z_t and \hat{z}_t can have unpredictable influence on policy making and can cause performance drop. To address this issue and minimize the uncertainty, we fuse the output from μ and ϕ with an adaptive ratio α to allow the policy network optimized jointly with the student network:

$$\begin{aligned} z'_t &= \alpha \hat{z}_t + (1 - \alpha) z_t \\ a_t &= \pi(z'_t, o_t) \end{aligned}$$

We update α with the progression of policy optimization. In the early stage, we set $\alpha = 0$ to train π by leveraging the privilege information encoded by μ . With the training going on, we gradually increase α , until only \hat{z}_t is used for policy making in the late stage. Thus, even if we cannot get a perfect replicate of z_t , π can still have the chance to learn to adapt

to such difference in a single phase to maximize the reward with the student network.

For training the adaption jointly in a single phase, we append the PPO optimization loss \mathcal{L}_{RL} [37] with $\mathcal{L}_{adaption}$, which is similar as [38]:

$$\mathcal{L} = \mathcal{L}_{RL} + \beta \mathcal{L}_{adaption}$$

The adaptive ratio β is negatively correlated to α . As the proportion of the student adaptor increases for policy making, we can focus more on the reward benefits instead of mimicking the teacher's behaviours.

During the deployment, the teacher model is pruned and the policy only relies on the student's adaption result $z'_t = \hat{z}_t$ in an asynchronous manner. The student model updates z' at a much slower frequency, as the real-world environment generally does not change rapidly under the desired locomotion speed [7].

C. Joint Locking Simulation

Joint failure for quadrupeds is common during the deployment in uncontrolled environments [21]. Joint locking and free swing are the most common faulty situations. A locked joint cannot be controlled freely and has only a limited range of motion. However, the actuator can still support the body as torques are still applied. A free swing joint cannot be controlled and no actions are made. It moves easily by an external force, thus cannot support the body. In this paper, we mainly consider the joint locking fault, since it can be possibly rectified by a fault-tolerant controller.

We model a joint locking failure by restricting the joint with a limited moving range $\theta_{allowed}$, controlled by a central position $\bar{\theta}$ and symmetrical tolerance θ_t :

$$\theta_{allowed} = [\bar{\theta} - \theta_t, \bar{\theta} + \theta_t]$$

When the failure happens, we directly overwrite the properties of the target joint in the simulator with the new upper limit and lower limit using the provided API in Isaac Gym [13]. In this way, we can get more true-to-life failure modeling without manually manipulating the output. Currently we focus on the single-joint failure scenario, since it is of much lower probability to have multiple faulty joints concurrently.

Joint Failure in the Simulation. In particular, to train a robust policy against joint locking accidents, we need to randomize such failure event to mimic the real-world situation. However, joint locking directly affects the joint control in a much more distinct way as the control profile is different. Furthermore, the status of the robot on the failing moment can alter the result. To simulate different dynamics when joint locking happens, we choose the online randomization strategy, where the failure happens randomly during each rollout for better coverage of the potential situations.

For each agent, we issue a failure flag $f_t \in [0, 12]$ to indicate the status of locking. Initially and after every reset, this flag is cleared for a normal state: $f_t = 0$. During the reset, the agent's failing timestep T_f is sampled after half of the maximum episode length following a continuous uniform distribution:

$$T_f \sim \mathcal{U}(0.5, 1.0) * T_{max}$$

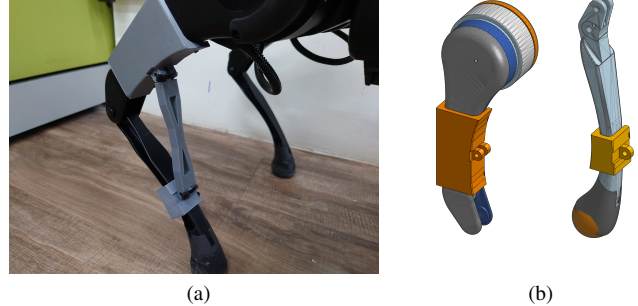


Fig. 3. The 3D-printed joint locking mechanism assembled in the physical device (a), containing two mounts for thigh link and calf link (b) for rod connection to form a locking situation.

and the locked joint is randomly selected from a discrete uniform distribution:

$$J_f \sim \mathcal{U}\{1, \dots, 12\}$$

When the progress of the agent t reaches the desired T_f , failure happens and f_t is updated to reflect the failing joint $f_t = J_f$. The current position of the select joint J_t is used as the central failure angle $\bar{\theta} = q_{J_t}$. The tolerance is sampled from a normal distribution with $\sigma = 0.05$ for updating joint properties.

We only pass the failure status flag f_t to the teacher model for training the environmental encoder ϕ as the joint position information already exists in o_t .

Joint Failure in the Real World. Quadrupedal robots are complex machines and modifying the hardware can be dangerous without the support from the manufacturer. For safety concerns, we design and 3D-printed an external locking mechanism (Fig. 3) to simulate the joint locking failure in the real world. It contains two mounting parts for calf and thigh link, and one adjustable-length rod in between, forming a strong structure to limit the motion. There are three joints on one leg and we choose calf as the failure target, as it is exposed in the open space and easy to work with. During the deployment, the mounting parts are attached to the robot link, while the rod is connected with zip-tie, which gives certain flexibility and can snap off if the torque is too large to avoid damaging the quadruped. The efficiency of the mechanism is evaluated in Section IV-C

D. Simulation Environment

Domain Randomization. This is a common method to bridge the sim-to-real gap, where key factors of the environment and robot are randomized in the simulator to ensure that the trained policy can handle different scenarios. Following [7], [9], we randomize the ground friction, PD controller settings, payload mass and CoM (the position to apply payload on the robot base body), motor strength and joint failure status (Section III-C). Table II summarizes the range of different randomized factors during training.

Terrain Generator and Curriculum: We use the terrain generator from [25] to simulate uneven terrains. Three types

TABLE II
DOMAIN RANDOMIZATION PARAMETERS

Factor	Range	Unit
Friction	[0.05, 4.5]	-
K_p	[50, 60]	-
K_d	[0.4, 0.8]	-
Payload Mass	[0, 6]	kg
Payload CoM	[-0.1, 0.1]	m
Motor Strength	[90, 110]	%
Failure Joint	{0, ..., 12}	-

of terrains are included in our simulation: 1) roughed sloped terrain; 2) smooth sloped terrain; 3) flat terrain with discrete obstacles. The terrains are generated with a curriculum strategy. Specifically, each type of terrain has 10 levels, with the increased difficulty (larger slope, larger roughness and higher obstacles). We track the assigned level of each agent and update the level based on the total travel distance during its lifespan. Despite the task is moving forward, the total distance is used as it indicates the basic maneuverability of the agent. If any agent has solved all the terrain levels, it will be looped back to level 1 for further exploration.

IV. EVALUATION

A. Implementation and Experimental Setup

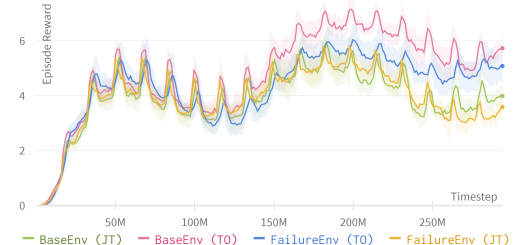
Module Implementation. Both the teacher model μ and control policy ϕ are implemented in MLP with the hidden layers of [512, 256, 128] and [256, 128] respectively, and the ELU activation. The teacher model outputs the latent representation with the length of $D = 8$. The student models follows [7] to adopt 1D CNNs for capturing temporal information with the history length $H = 50$ followed by a linear projection to the same latent space. We optimize all the models jointly with PPO [37] to maximize the future discounted reward.

Simulation. Isaac Gym and its open-sourced library IsaacGymEnvs [13] are used to simulate massive parallel environments on rough terrains based on the sample code from [25]. The back-end PhysX [39] physical engine runs at 400Hz for simulating the environment while our agent runs at 100 Hz for information collection and processing. We run the simulation on two NVIDIA A6000 GPUs, each handling 4096 environments, which can provide over 0.1M FPS for simulation. We collect 300M simulated steps of equivalently 35 real days of experience in 40 minutes of wall-clock time.

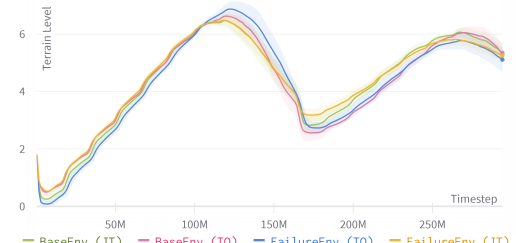
Hardware. We adopt Unitree A1 as the test platform for the experiments. A1 is a low-cost quadruped driven by 12 direct-drive actuators, each paired with one 15-bit encoder, providing precise joint position and velocity measurement. We additionally access onboard IMU and foot-end force sensors for gravity vector of the base body and the binarized contact indicator used by our adaption network for state prediction. We use an external NVIDIA Jetson Xavier NX to replace the onboard Raspberry Pi high-level controller for additional GPU acceleration to process the exported JIT model.

B. Simulation Results

We implement two virtual environments in Isaac Gym: a basic environment similar to [7] (BaseEnv) and a faulty



(a)



(b)

Fig. 4. We train each model 5 times with random seeds. (a) shows the average reward during the training progress. (b) shows the average terrain level. Due to the loop back curriculum strategy, the levels show a wave form.

TABLE III
PERFORMANCE OF THE TRAINED AGENT IN THE SIMULATOR

Environment	Accumulated reward		Average speed (m/s)	
	TO	JT	TO	JT
BaseEnv	8.90	8.68	0.73	0.63
FailureEnv	8.38	8.20	0.61	0.60

environment where the joint locking failure randomly happens (FailureEnv). To demonstrate the joint training (JT) efficiency, we train an additional teacher-only (TO) agent in each environment, which represents the best possible performance under the same iterations. Fig. 4 shows the average accumulated reward and average terrain level during training. We observe that BaseEnv has an overall slightly better performance than FailureEnv, which is expected due to the impact of joint locking.

For joint training, the student model starts to contribute to the policy at timestep 60M, even before most TO agents solve all the terrain levels at around 120M. In the last 100M timestep the training only focuses on the student and policy networks for maximizing reward to avoid being influenced by the under-laying privilege state. The resulted JT agents slightly underperform the TO agents due to the loss of privilege information. However, such performance drop is acceptable on the quadruped locomotion. We deploy the trained agents in simulator for inference. Table III shows the final accumulated reward and average speed for two environments with TO and JT training, respectively. We can observe that the JT training can obtain satisfactory performance for practical deployment.



Fig. 5. Deployment result on physical robot. (a) shows a normal run without any joint failure. (b) shows the `FailureEnv` agent can still run even with one joint locked. (c) shows the `BaseEnv` agent cannot handle joint locking failure and immediately fails. The safety rope is only used for preventing hardware damage and will not affect the running. Please refer to our supplementary video for more information.

C. Physical Validation

We convert the trained model to JIT and deploy it directly on the physical Unitree device for a zero-shot transfer without any fine-tuning. We follow the asynchronous deployment where the policy model runs at 100Hz while the adaption module runs at 10Hz for updating \hat{z} . We compare the performance between the baseline model trained under `BaseEnv` and the built-in A1 controller. For safety concerns, we only run the controller for a limited time and the trajectory is tracked by an indoor ultra-wideband (UWB) system.

Fig. 5 compares the running actions of different agents (the built-in A1 controller, `BaseEnv`, and our `FailureEnv`). When one joint is locked, both the built-in A1 controller and `BaseEnv` agents fail to effectively control the quadruped, making it directly fall on the ground, where human assistant is needed for recovery (Fig. 5c). For the `FailureEnv` agent, it travels forward at an average speed of 0.82 m/s with almost no lateral offset under the normal situation (Fig. 5a). With one joint locked, it can still maintain heading at an average speed of 0.39 m/s, almost half of the normal speed (Fig. 5b).

Additionally, to validate the joint locking mechanism, we compare the joint movement and velocity before and after the joint is locked (Fig. 6). The locking mechanism can efficiently limit the movement of the joint to simulate the failure situation in the real world.

V. CONCLUSION AND FUTURE WORK

In this paper, we propose the first methodology to train hardware fault-tolerant RL-based controller for quadruped locomotion. We design a novel strategy for joint locking failure simulation. A joint training pipeline is further developed

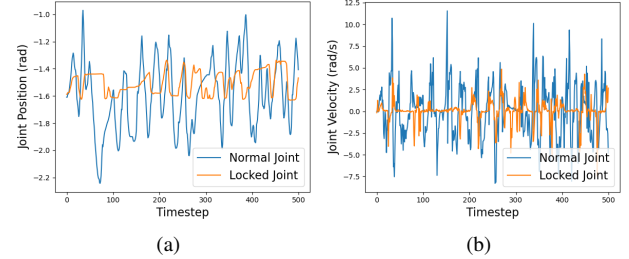


Fig. 6. We track the position (a) and velocity (b) of the locked joint on the physical quadruped during testing.

for fault-tolerant quadruped locomotion controller upon the teacher-student framework. We use commonly used low-level sensors available on quadrupedal robots as the observations to generate the robust actions. We demonstrate that even with one joint locked, our controller can still drive the quadruped without losing too much heading or speed.

Quadrupedal robot failure is a complex topic and depends on the robot specifications. Delicate simulation and training are needed to be truly robust against all situations. Due to safety concerns, we currently only conduct experiments with forward movement, which can be further extended with additional user command input for controllable locomotion deployment. To further improve the fault tolerance of the locomotion controller, we will develop a unified and transferable solution for a variety of quadrupedal robotics platform with different morphology, dynamics and sensor sets. We can further couple with additional high-level sensors like depth cameras for safe and reliable task-related deployment.

REFERENCES

[1] E. Krotkov, D. Hackett, L. Jackel, M. Perschbacher, J. Pippine, J. Strauss, G. Pratt, and C. Orlowski, “The darpa robotics challenge finals: Results and perspectives,” in *The DARPA Robotics Challenge Finals: Humanoid Robots To The Rescue*. Springer, 2018, pp. 1–26.

[2] C. D. Bellicoso, M. Bjelonic, L. Wellhausen, K. Holtmann, F. Günther, M. Tranzatto, P. Fankhauser, and M. Hutter, “Advances in real-world applications for legged robots,” *Journal of Field Robotics*, vol. 35, no. 8, pp. 1311–1326, 2018.

[3] Z. Chen, T. Fan, X. Zhao, J. Liang, C. Shen, H. Chen, D. Manocha, J. Pan, and W. Zhang, “Autonomous social distancing in urban environments using a quadruped robot,” *IEEE Access*, vol. 9, pp. 8392–8403, 2021.

[4] J. Hooks, M. S. Ahn, J. Yu, X. Zhang, T. Zhu, H. Chae, and D. Hong, “Alphred: A multi-modal operations quadruped robot for package delivery applications,” *IEEE Robotics and Automation Letters*, vol. 5, no. 4, pp. 5409–5416, 2020.

[5] T. Miki, J. Lee, J. Hwangbo, L. Wellhausen, V. Koltun, and M. Hutter, “Learning robust perceptive locomotion for quadrupedal robots in the wild,” *Science Robotics*, vol. 7, no. 62, p. eabk2822, 2022.

[6] J. Lee, J. Hwangbo, L. Wellhausen, V. Koltun, and M. Hutter, “Learning quadrupedal locomotion over challenging terrain,” *Science robotics*, vol. 5, no. 47, p. eabc5986, 2020.

[7] A. Kumar, Z. Fu, D. Pathak, and J. Malik, “RMA: rapid motor adaptation for legged robots,” in *Robotics: Science and Systems XVII, Virtual Event, July 12–16, 2021*, 2021.

[8] H.-W. Park, P. M. Wensing, and S. Kim, “Jumping over obstacles with mit cheetah 2,” *Robotics and Autonomous Systems*, vol. 136, p. 103703, 2021.

[9] G. Margolis, G. Yang, K. Paigwar, T. Chen, and P. Agrawal, “Rapid locomotion via reinforcement learning,” in *Robotics: Science and Systems*, 2022.

[10] F. Shi, T. Homberger, J. Lee, T. Miki, M. Zhao, F. Farshidian, K. Okada, M. Inaba, and M. Hutter, “Circus anomal: A quadruped learning dexterous manipulation with its limbs,” in *2021 IEEE International Conference on Robotics and Automation (ICRA)*. IEEE, 2021, pp. 2316–2323.

[11] J. Di Carlo, P. M. Wensing, B. Katz, G. Bledt, and S. Kim, “Dynamic locomotion in the mit cheetah 3 through convex model-predictive control,” in *2018 IEEE/RSJ international conference on intelligent robots and systems (IROS)*. IEEE, 2018, pp. 1–9.

[12] C. Gehring, S. Coros, M. Hutter, C. D. Bellicoso, H. Heijnen, R. Diethelm, M. Bloesch, P. Fankhauser, J. Hwangbo, M. Hoepflinger *et al.*, “Practice makes perfect: An optimization-based approach to controlling agile motions for a quadruped robot,” *IEEE Robotics & Automation Magazine*, vol. 23, no. 1, pp. 34–43, 2016.

[13] V. Makovychuk, L. Wawrzyniak, Y. Guo, M. Lu, K. Storey, M. Macklin, D. Hoeller, N. Rudin, A. Allshire, A. Handa *et al.*, “Isaac gym: High performance gpu-based physics simulation for robot learning,” *arXiv preprint arXiv:2108.10470*, 2021.

[14] J. Tobin, R. Fong, A. Ray, J. Schneider, W. Zaremba, and P. Abbeel, “Domain randomization for transferring deep neural networks from simulation to the real world,” in *2017 IEEE/RSJ international conference on intelligent robots and systems (IROS)*. IEEE, 2017, pp. 23–30.

[15] X. B. Peng, M. Andrychowicz, W. Zaremba, and P. Abbeel, “Sim-to-real transfer of robotic control with dynamics randomization,” in *2018 IEEE international conference on robotics and automation (ICRA)*. IEEE, 2018, pp. 3803–3810.

[16] J. Hwangbo, J. Lee, A. Dosovitskiy, D. Bellicoso, V. Tsounis, V. Koltun, and M. Hutter, “Learning agile and dynamic motor skills for legged robots,” *Science Robotics*, vol. 4, no. 26, p. eaau5872, 2019. [Online]. Available: <https://www.science.org/doi/abs/10.1126/scirobotics.aau5872>

[17] Y. Zhong, R. Wang, H. Feng, and Y. Chen, “Analysis and research of quadruped robot’s legs: A comprehensive review,” *International Journal of Advanced Robotic Systems*, vol. 16, no. 3, p. 1729881419844148, 2019.

[18] J.-M. Yang, “Kinematic constraints on fault-tolerant gaits for a locked joint failure,” *Journal of Intelligent and Robotic Systems*, vol. 45, no. 4, pp. 323–342, 2006.

[19] C. Pana, I. Resceanu, and D. Patrascu, “Fault-tolerant gaits of quadruped robot on a constant-slope terrain,” in *2008 IEEE International Conference on Automation, Quality and Testing, Robotics*, vol. 1. IEEE, 2008, pp. 222–226.

[20] M. Gor, P. M. Pathak, A. Samantaray, J.-M. Yang, and S. Kwak, “Fault accommodation in compliant quadruped robot through a moving appendage mechanism,” *Mechanism and Machine Theory*, vol. 121, pp. 228–244, 2018.

[21] J. Cui, Z. Li, J. Qiu, and T. Li, “Fault-tolerant motion planning and generation of quadruped robots synthesised by posture optimization and whole body control,” *Complex & Intelligent Systems*, pp. 1–13, 2022.

[22] W. Okamoto, H. Kera, and K. Kawamoto, “Reinforcement learning with adaptive curriculum dynamics randomization for fault-tolerant robot control,” *arXiv preprint arXiv:2111.10005*, 2021.

[23] J. Di Carlo, P. M. Wensing, B. Katz, G. Bledt, and S. Kim, “Dynamic locomotion in the mit cheetah 3 through convex model-predictive control,” in *2018 IEEE/RSJ International Conference on Intelligent Robots and Systems (IROS)*, 2018, pp. 1–9.

[24] M. Neunert, M. Stäuble, M. Gifthaler, C. D. Bellicoso, J. Carius, C. Gehring, M. Hutter, and J. Buchli, “Whole-body nonlinear model predictive control through contacts for quadrupeds,” *IEEE Robotics and Automation Letters*, vol. 3, pp. 1458–1465, 2018.

[25] N. Rudin, D. Hoeller, P. Reist, and M. Hutter, “Learning to walk in minutes using massively parallel deep reinforcement learning,” in *Conference on Robot Learning*. PMLR, 2022, pp. 91–100.

[26] E. Vollenweider, M. Bjelonic, V. Klemm, N. Rudin, J. Lee, and M. Hutter, “Advanced skills through multiple adversarial motion priors in reinforcement learning,” *arXiv preprint arXiv:2203.14912*, 2022.

[27] S. Koos, J.-B. Mouret, and S. Doncieux, “Crossing the reality gap in evolutionary robotics by promoting transferable controllers,” in *Proceedings of the 12th annual conference on Genetic and evolutionary computation*, 2010, pp. 119–126.

[28] A. Boeing and T. Bräunl, “Leveraging multiple simulators for crossing the reality gap,” in *2012 12th international conference on control automation robotics & vision (ICARCV)*. IEEE, 2012, pp. 1113–1119.

[29] J. Tan, T. Zhang, E. Coumans, A. Iscen, Y. Bai, D. Hafner, S. Bohez, and V. Vanhoucke, “Sim-to-real: Learning agile locomotion for quadruped robots,” in *Robotics: Science and Systems*, 2018.

[30] A. Loquercio, E. Kaufmann, R. Ranftl, A. Dosovitskiy, V. Koltun, and D. Scaramuzza, “Deep drone racing: From simulation to reality with domain randomization,” *IEEE Transactions on Robotics*, vol. 36, no. 1, pp. 1–14, 2019.

[31] O. M. Andrychowicz, B. Baker, M. Chociej, R. Jozefowicz, B. McGrew, J. Pachocki, A. Petron, M. Plappert, G. Powell, A. Ray *et al.*, “Learning dexterous in-hand manipulation,” *The International Journal of Robotics Research*, vol. 39, no. 1, pp. 3–20, 2020.

[32] Y. Chebotar, A. Handa, V. Makovychuk, M. Macklin, J. Issac, N. Ratliff, and D. Fox, “Closing the sim-to-real loop: Adapting simulation randomization with real world experience,” in *2019 International Conference on Robotics and Automation (ICRA)*. IEEE, 2019, pp. 8973–8979.

[33] W. Yu, J. Tan, C. K. Liu, and G. Turk, “Preparing for the unknown: Learning a universal policy with online system identification,” *arXiv preprint arXiv:1702.02453*, 2017.

[34] G. B. Margolis, T. Chen, K. Paigwar, X. Fu, D. Kim, S. bae Kim, and P. Agrawal, “Learning to jump from pixels,” in *5th Annual Conference on Robot Learning*, 2021.

[35] Y. Tassa, Y. Doron, A. Muldal, T. Erez, Y. Li, D. d. L. Casas, D. Budden, A. Abdolmaleki, J. Merel, A. Lefrancq *et al.*, “Deepmind control suite,” *arXiv preprint arXiv:1801.00690*, 2018.

[36] M. Laskin, A. Srinivas, and P. Abbeel, “Curl: Contrastive unsupervised representations for reinforcement learning,” in *International Conference on Machine Learning*. PMLR, 2020, pp. 5639–5650.

[37] J. Schulman, F. Wolski, P. Dhariwal, A. Radford, and O. Klimov, “Proximal policy optimization algorithms,” 2017. [Online]. Available: <https://arxiv.org/abs/1707.06347>

[38] H. Wu, K. Khetarpal, and D. Precup, “Self-supervised attention-aware reinforcement learning,” in *Proceedings of the AAAI Conference on Artificial Intelligence*, vol. 35, no. 12, 2021, pp. 10311–10319.

[39] “Nvidia physx 4.5 and 5.0 sdk,” Aug 2022. [Online]. Available: <https://developer.nvidia.com/physx-sdk>